Energy 39 (2012) 310–318

Contents lists available at SciVerse ScienceDirect

Energy

journal homepage: www.elsevier.com/locate/energy

Online model-based estimation of state-of-charge and open-circuit voltage of lithium-ion batteries in electric vehicles

Hongwen He*, Xiaowei Zhang, Rui Xiong, Yongli Xu, Hongqiang Guo

National Engineering Laboratory for Electric Vehicles, School of Mechanical Engineering, Beijing Institute of Technology, South No. 5 Zhongguancun Street, Beijing 100081, China

ARTICLE INFO

Article history:
Received 9 October 2011
Received in revised form
3 January 2012
Accepted 4 January 2012
Available online 4 February 2012

Keywords:
State-of-charge
Open-circuit voltage
Equivalent circuit model
Online estimation
Electric vehicles

ABSTRACT

This paper presents a method to estimate the state-of-charge (SOC) of a lithium-ion battery, based on an online identification of its open-circuit voltage (OCV), according to the battery's intrinsic relationship between the SOC and the OCV for application in electric vehicles. Firstly an equivalent circuit model with *n* RC networks is employed modeling the polarization characteristic and the dynamic behavior of the lithium-ion battery, the corresponding equations are built to describe its electric behavior and a recursive function is deduced for the online identification of the OCV, which is implemented by a recursive least squares (RLS) algorithm with an optimal forgetting factor. The models with different RC networks are evaluated based on the terminal voltage comparisons between the model-based simulation and the experiment. Then the OCV-SOC lookup table is built based on the experimental data performed by a linear interpolation of the battery voltages at the same SOC during two consecutive discharge and charge cycles. Finally a verifying experiment is carried out based on nine Urban Dynamometer Driving Schedules. It indicates that the proposed method can ensure an acceptable accuracy of SOC estimation for online application with a maximum error being less than 5.0%.

1. Introduction

The battery pack, as a key component, is crucial for the performance of electric vehicles (EVs), such as economy, power performance, security, etc. It is significant to accurately manage the battery pack to extend its lifespan, improve its reliability and lower its cost. Usually state-of-charge (SOC) and state-of health (SOH) are used to denote the usable energy and the usable lifespan of the battery pack respectively [1,2]. The online estimation of SOC and SoH, which is also vital for the power distribution strategy of EVs, is one of the main tasks of the battery management system (BMS). Various kinds of battery models are built for the model-based estimation of SOC and SoH [3–5]. By comparison, the equivalent circuit models, which consist of resistors, capacitors and voltage sources, are widely used simulating the battery pack's operation performance. For example, the Rint model is used and verified in the simulation software Advisor [6], however, a bad dynamic simulation is performed due to the ignorance of the relaxation effect; The Thevenin model achieves a big improvement by connecting a parallel RC network in series on the basis of the Rint model simulating the polarization characteristic [7,8]; An improved model is proposed and verified with higher accuracy by connecting an additional parallel RC network in series based on the Thevenin model simulating the concentration polarization and the electrochemical polarization separately [9]. For the battery's complicated polarization characteristic, some studies deduce and suggest that the models with more parallel RC networks connected in series should have much higher accuracy [10], however, at the same time, memory consumption, waste calculation and bad real-time application are caused. Since most of the high-accuracy battery models are built with the preconditions of offline simulation and well-controlled laboratory environment, there still need much improvement for the online applications in EVs.

The existed SOC estimation methods can be generally categorized into direct kind and indirect kind. One of the direct approaches simply indicates the remaining capacity by using an online current integration. However, a big SOC estimation error exists caused by the inaccurate initial SOC and the low calculation accuracy of the Ah consumption due to some uncertain disturbances. Some studies improve the accuracy by compensating for efficiency, temperature and aging effects and revise the initial SOC periodically according to the open-circuit voltage (OCV) [11].

On the other hand, the indirect methods determine the SOC by using the battery's intrinsic relationship between the SOC and some

* Corresponding author. Tel./fax: +86 10 6891 4842.
E-mail addresses: hwhebit@bit.edu.cn, hwenhe@263.net (H. He).

0360-5442/$ – see front matter © 2012 Elsevier Ltd. All rights reserved.
doi:10.1016/j.energy.2012.01.009

electrical parameters such as the OCV [12–14]. The OCV naturally declines proportionately with the energy expenditure and is widely used for SOC estimation. But the direct measurement of the OCV is difficult for online application due to the long waiting time for the batteries to reach a steady state [15,16]. Another indirect method is based on state estimation techniques with state-space battery models [17,18]. The extended kalman filter (EKF) is popularly selected for SOC estimation due to the advantages of being close-loop and available to regulate the estimation error range dynamically [19]. However, it strongly depends on the accuracy of the battery model as well as the predetermined variables of the system noise such as mean value, pertinence and covariance matrix. An improper setting of the predetermined variables of the system noise may result in remarkable errors and divergence.

A model-based, online estimation method of SOC and OCV of a lithium-ion battery module is put forward in this paper. The research proceeds as following: an equivalent circuit model with n RC networks is built modeling the relaxation effect and the dynamic behavior of the batteries; Then, a recursive least squares (RLS) algorithm with an optimal forgetting factor is applied to implement the online identification of the model parameters; An evaluation among the models with different RC networks is carried out and a suitable model is selected with enough accuracy and low calculation cost; Based on the selected model, the online estimation of the equivalent ohmic resistance and the OCV is conducted, and then the lookup table between the OCV and the SOC is built by experimental approach; Finally, a verifying experiment is carried out based on several consecutive Urban Dynamometer Driving Schedules (UDDS).

2. Equivalent circuit model of lithium-ion batteries

For lithium-ion batteries, based on an analysis on the structure of the Rint model and the Thevenin model broadly used, an equivalent circuit model with n RC networks, named the NP model hereafter, is built which is shown in Fig. 1. Where I_L is the load current with a positive value in the discharge process and a negative value in the charge process, U_L is the terminal voltage, U_{OC} is the OCV, R_O is the equivalent ohmic resistance, C_i is the ith equivalent polarization capacitance and R_i is the ith equivalent polarization resistance simulating the transient response during a charge or discharge process, U_i is the voltage across C_i. $i = 1,2,3,4,\ldots n$. The electrical behavior of the NP model can be expressed by Eq. (1) in the frequency domain.

$$U_L(s) = U_{OC}(s) - I_L(s)\left(R_O + \frac{R_1}{1+R_1C_1s} + \cdots + \frac{R_n}{1+R_nC_ns}\right) \quad (n = 0,1,2\cdots) \tag{1}$$

Where s is the frequency operator.

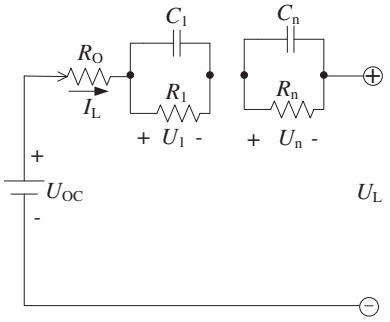

Fig. 1. Schematic diagram of the NP model.

2.1. In case of $n = 0$

The NP model is simplified as the Rint model and a discretization form of Eq. (1) is written as Eq. (2), where k denotes the discretization step with a sample interval of T, $k = 1,2,3,\ldots$.

$$U_L(k) = U_{OC}(k) - R_OI_L(k) \tag{2}$$

Define $\varphi_0(k) = [1 \quad I_L(k)]$, $\theta_0(k) = [U_{OC}(k) \quad -R_O]^T$, then,

$$y_k = \varphi_0(k)\theta_0(k) \tag{3}$$

2.2. In case of $n = 1$

The NP model is simplified as the Thevenin model and then,

$$U_L(s) - U_{OC}(s) = -I_L(s)\left(R_O + \frac{R_1}{1+R_1C_1s}\right) \tag{4}$$

Define $E_L = U_L - U_{OC}$, the transfer function $G(s)$ of Eq. (4) can be written as Eq. (5).

$$G(s) = \frac{E_L(s)}{I_L(s)} = -R_O - \frac{R_1}{1+R_1C_1s} = -\frac{R_O + R_1 + R_OR_1C_1s}{1+R_1C_1s} \tag{5}$$

A bilinear transformation method shown in Eq. (6) is employed for the discretization calculation of Eq. (5) and the result is shown in Eq. (7).

$$s = \frac{2}{T}\frac{1-z^{-1}}{1+z^{-1}} \tag{6}$$

Where z is the discretization operator.

$$G\left(z^{-1}\right) = -\frac{\frac{R_0T + R_1T + 2R_0R_1C_1}{T+2R_1C_1} + \frac{R_0T + R_1T - 2R_0R_1C_1}{T+2R_1C_1}z^{-1}}{1 + \frac{T-2R_1C_1}{T+2R_1C_1}z^{-1}} \tag{7}$$

Define $a_1 = -\frac{T-2R_1C_1}{T+2R_1C_1}$, $a_2 = -\frac{R_0T + R_1T + 2R_0R_1C_1}{T+2R_1C_1}$ and $a_3 = -\frac{R_0T + R_1T - 2R_0R_1C_1}{T+2R_1C_1}$, then R_O can be solved according to the united equations of a_1, a_2 and a_3.

$$R_0 = \frac{T(a_3 - a_2)}{T + a_1} \tag{8}$$

Eq. (4) is rewritten as Eq. (9) after discretization, where $k = 1,2,3,\ldots$.

$$E_L(k) = a_1E_L(k-1) + a_2I_L(k) + a_3I_L(k-1) \tag{9}$$

The OCV is greatly influenced by SOC, working temperature *Tem* and working history H, which are all the functions of time t, herein we define the OCV as a function of SOC, *Tem* and H shown in Eq. (10).

$$U_{OC} = f(\mathrm{SOC}(t), \mathrm{Tem}(t), H(t)) \tag{10}$$

Differentiate U_{OC} in Eq. (10) with respect to time t.

$$\frac{dU_{OC}}{dt} = \frac{\partial U_{OC}}{\partial \mathrm{SOC}}\frac{\partial \mathrm{SOC}}{\partial t} + \frac{\partial U_{OC}}{\partial Tem}\frac{\partial \mathrm{Tem}}{\partial t} + \frac{\partial U_{OC}}{\partial H}\frac{\partial H}{\partial t} \tag{11}$$

Eq. (11) can be simplified as Eq. (12) after considering the following assumptions [12]: The $\partial \mathrm{SOC}/\partial t \approx 0$ holds for small battery energy is consumed or regained relative to totally useable capacity; Relying on the proper design of a cooling system/heater of BMS, the temperature rise/decrease of batteries should be slow, the

$\partial Tem/\partial t \approx 0$ holds for normal operating conditions; The $\partial H/\partial t \approx 0$ definitely holds since H represents a long usage history.

$$\frac{dU_{OC}}{dt} = \frac{U_{OC}(k) - U_{OC}(k-1)}{T} \approx 0 \tag{12}$$

$$\Delta U_{OC}(k) = U_{OC}(k) - U_{OC}(k-1) \approx 0 \tag{13}$$

And then Eq. (9) is rewritten as Eq. (14).

$$U_L(k) = (1-a_1)U_{oc}(k) + a_1 U_L(k-1) + a_2 I_L(k) + a_3 I_L(k-1) \tag{14}$$

Define $\varphi_1(k) = [1 \;\; U_L(k-1) \;\; I_L(k) \;\; I_L(k-1)]$,

$\theta_1(k) = [(1-a_1)U_{OC}(k) \;\; a_1 \;\; a_2 \;\; a_3]^T$ and $y_k = U_L(k)$, then,

$$y_k = \phi_1(k)\theta_1(k) \tag{15}$$

In case of online application, the $U_L(k)$ and $I_L(k)$ are sampled at constant period, the vector θ_1 can be identified by a recursive least squares algorithm according to Eq. (15),and then the model parameters can be solved by the expressions of a_1,a_2,a_3.

2.3. In case of $n = 2$

The NP model is simplified and then,

$$E_L(s) = -I_L(s)\left(R_O + \frac{R_1}{1+R_1C_1s} + \frac{R_2}{1+R_2C_2s}\right) \tag{16}$$

The corresponding transfer function $G(s)$ of Eq. (16) is.

$$G(s) = -\frac{R_0s^2 + \frac{1}{R_1C_1R_2C_2}(R_OR_1C_1 + R_OR_2C_2 + R_2R_1C_1 + R_1R_2C_2)\,s + \frac{R_O+R_1+R_2}{R_1C_1R_2C_2}}{s^2 + \frac{R_1C_1+R_2C_2}{R_1C_1R_2C_2}s + \frac{1}{R_1C_1R_2C_2}} \tag{17}$$

The bilinear transformation method shown in Eq. (6) is employed for the discretization calculation of Eq. (17), then,

$$G\left(z^{-1}\right) = \frac{b_3 + b_4z^{-1} + b_5z^{-2}}{1 - b_1z^{-1} - b_2z^{-2}} \tag{18}$$

Where b_1, b_2, b_3, b_4 and b_5 are the coefficients solved from Eq. (17).

Similar to the case of $n = 1$, a discretization form of Eq. (16) is arranged as Eq. (19), where $k = 2,3,4\ldots..$

$$\begin{aligned} U_L(k) = {} & (1-b_1-b_2)U_{OC}(k) + b_1U_L(k-1) + b_2U_L(k-2) \\ & + b_3I_L(k) + b_4I_L(k-1) + b_5I_L(k-2) \end{aligned} \tag{19}$$

Define $\varphi_2(k) = [1 \;\; U_L(k-1) \;\; U_L(k-2) \;\; I_L(k) \;\; I_L(k-1) \;\; I_L(k-2)]$,

$y_k = U_L(k)$ and $\theta_2(k) = [(1-b_1-b_2)U_{OC} \;\; b_1 \;\; b_2 \;\; b_3 \;\; b_4 \;\; b_5]^T$, then,

$$y_k = \varphi_2(k)\theta_2(k) \tag{20}$$

In case of online application, the $U_L(k)$ and $I_L(k)$ are sampled at constant period, the vector θ_2 can be identified by a RLS algorithm according to Eq. (20),and the model parameters can be solved by Eq. (21).

$$\begin{cases} R_O = \dfrac{-b_3+b_4-b_5}{1+b_1-b_2} \\ R_1C_1R_2C_2 = \dfrac{-b_3+b_4-b_5}{1-b_1-b_2} \\ R_1C_1 + R_2C_2 = \dfrac{T(1+b_2)}{1-b_1-b_2} \\ R_O + R_1 + R_2 = \dfrac{-b_3+b_4-b_5}{1-b_1-b_2} \\ R_OR_1C_1 + R_OR_2C_2 + R_2R_1C_1 + R_1R_2C_2 = \dfrac{4(b_5-b_3)}{T(1+b_1-b_2)} \end{cases} \tag{21}$$

2.4. In case of $n = n$

The electrical behavior of the NP model is deduced and written as Eq. (22).

$$E_L(s) = -I_L(s)\left(\frac{R_1}{1+R_1C_1s} + \frac{R_2}{1+R_2C_2s} + \cdots + \frac{R_n}{1+R_nC_ns} + R_O\right) \tag{22}$$

The bilinear transformation method shown in Eq. (6) is employed for the discretization of Eq. (22), and Eq. (23) is deduced according to Eq. (14) and Eq. (19), where $k = n, n+1, n+2,\ldots.$

$$\begin{aligned} U_L(k) = {} & \left(1 - \sum_{i=1}^{n} c_i\right)U_{OC}(k) + c_1U_L(k-1) + c_2U_L(k-2) + \ldots \\ & + c_nU_L(k-n) + c_{n+1}I_L(k) + c_{n+2}I_L(k-1) + \ldots \\ & + c_{2n+1}I_L(k-n) \end{aligned} \tag{23}$$

Similarly, a recursive function is built as Eq. (24) with the input vector $\varphi_n(k)$, parameters vector $\theta_n(k)$ and the outputy$_k = U_L(k)$.

$$y_k = \varphi_n(k)\theta_n(k) \tag{24}$$

$$\varphi_n(k) = [1 \quad U_L(k-1) \quad U_L(k-2) \quad \cdots \quad U_L(k-n) \quad I_L(k-1) \quad I_L(k-2) \quad \cdots I_L(k-n)] \tag{25}$$

$$\theta_n(k) = \left[\left(1 - \sum_{i=1}^{n} c_i\right)U_{OC}(k)\; c_1 \quad c_2 \quad c_3 \quad \cdots \quad c_{2n+1}\right]^T \tag{26}$$

It can be seen that the model parameters will increase manifoldly with the increase of the number of RC networks, and the calculation burden will be heavier and a larger memory will be required to store the large amount of sample data. It is meaningful to properly select a minimum RC networks with an acceptable accuracy.

3. Identification algorithm of the model parameters

The conventional system identification techniques such as RLS method do not always give exact or good quality model of a dynamic system compared with other techniques such as Genetic algorithm, those approaches based on kalman filter and neural networks [19,20]. However, with some modifications and improvements, the RLS can also benefit and result in an optimization system model. The problem of standard RLS is that it leads to

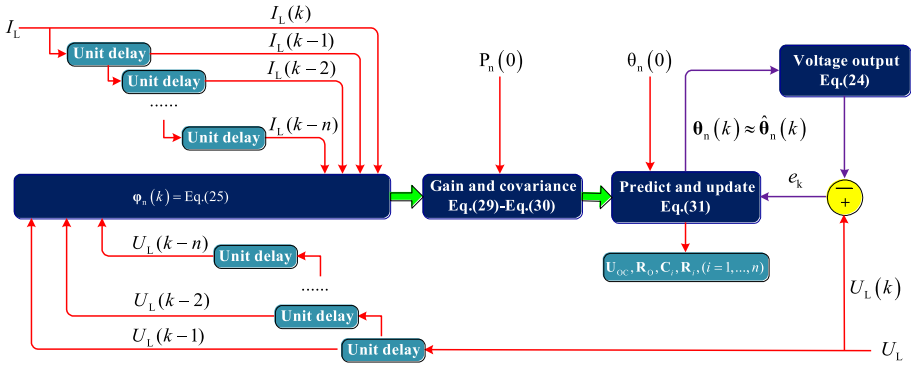

Fig. 2. Scheme of the identification of the NP model parameters.

the saturation phenomenon. This drawback is due to the exponential growth of the covariance matrix. In this paper, based on the standard RLS method, an optimal forgetting factor is employed to give less weight to old data and more weight to recent data, the parameter estimate is updated at every sample intervals on the basis of current measurement at time kT and previous estimates at time $(k-1)T$ [21].

For the recursive function of Eq. (24), the system identification is realized as follows.

$$y_k = \varphi_n(k)\theta_n(k) + e(k) \tag{27}$$

$$e(k) = U_L(k) - \varphi_n(k)\hat{\theta}_n(k-1) \tag{28}$$

$$K(k) = \frac{P(k-1)\varphi_n^T(k)}{\lambda + \varphi_n^T(k)P(k-1)\varphi_n(k)} \tag{29}$$

$$P(k) = \frac{P(k-1) - K(k)\varphi_n^T(k)P(k-1)}{\lambda} \tag{30}$$

$$\hat{\theta}_n(k) = \hat{\theta}_n(k-1) + K(k)e(k) \tag{31}$$

Where $\hat{\theta}_n(k)$ is the estimate of the parameter vector θ_n, $e(k)$ is the prediction error of the terminal voltage, $\boldsymbol{K}(k)$ is the algorithm gain and $\boldsymbol{P}$(k) is the covariance matrix, the constant λ is the forgetting factor and is very important to obtain a good estimated parameter set with small error, typically $\lambda \in [0.95, 1]$.

The schematic diagram for the online identification of the NP battery model parameters is shown in Fig. 2. The initial values of the parameter vector $\theta_n(0)$ and its error covariance matrix $\boldsymbol{P}(0)$ are preset. Then, the parameter vector $\theta_n(k)$ can be adjusted adaptively according to the samples of $U_L(k)$,$I_L(k)$.

4. Experiments and online identification of model parameters

4.1. Test bench

The test bench is shown in Fig. 3, which consists of a Digatron battery test system EVT50-400, a BMS module, a CAN communication unit and a host computer with built-in BMS software for online experiment and BTS-600 interface for programming the EVT50-400. The host computer is used for the real-time calculation of the model parameters. The EVT50-400 can charge/discharge a battery pack according to the designed program with maximum voltage of 50 V and maximum charge/discharge current of 400 A, and its recorded data include current, voltage, temperature, accumulative Amp-hours (Ah) and Watt-hours (Wh) etc. The BMS module also samples the battery's voltages, current and temperatures. The errors of the Hall current and voltage sensors of BMS are less than 0.2% and 0.5% respectively. The measured data is transmitted to the host computer through USB and TCP/IP driven by the CAN communication unit and EVT50-400 respectively. Both the host computer and the BMS module have a low-pass filter to implement large noise cancellation [10]. Furthermore, in order to improve the sample precision of terminal voltages, the Fluke 8846A multimeter shown in Fig. 4, whose measurement accuracy of DC voltage is up to 0.0024% with a 6.5 digit resolution, has been applied for voltage measurement. As a result, the test bench has a current measurement accuracy of ±10 mA (EVT50-400) and

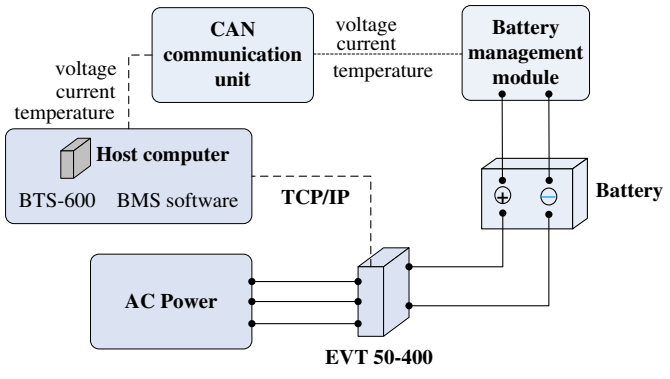

Fig. 3. Schematic of the battery test bench.

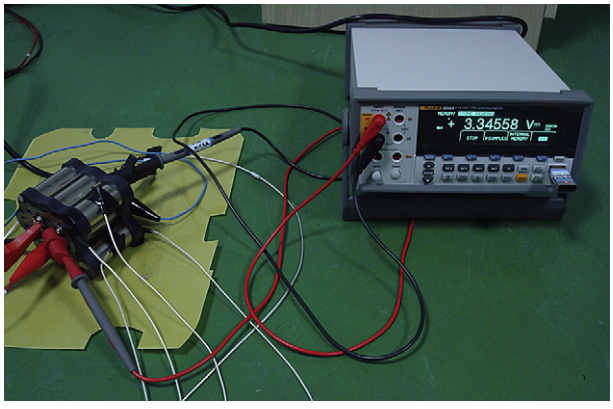

Fig. 4. Fluke 8846A test bench.

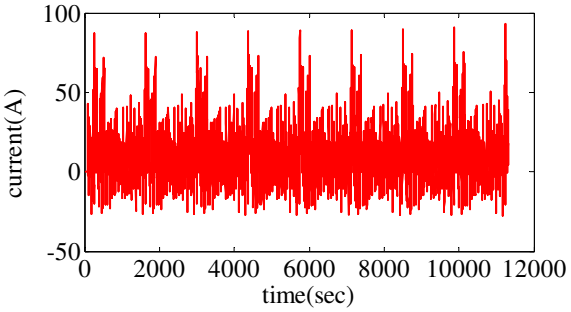

Fig. 5. The experimental load current profiles of 9 UDDS cycles.

voltage measurement accuracy of 0.0024% (Fluke 8846A multimeter, <0.1 mV for the battery module with a maximum voltage of 4.0 V). A $LiFePO_4$ battery module with nominal voltage of 3.2 V and nominal capacity of 27 Ah, which is constructed by 9 cells connected in parallel, is selected for the experiments. For each cell, its nominal capacity is 3 Ah and its nominal voltage is 3.2 V.

The Urban Dynamometer Driving Schedule (UDDS) test is a typical dynamic driving cycle which is often used to evaluate the performance of vehicle, control strategies of EVs, SOC estimation algorithms et al. [22,23]. In this paper nine consecutive UDDS cycles are employed to verify the online estimation approach. The sample interval is 1 s. For EVT50-400, UDDS test is performed with the current profiles shown in Fig. 5 and terminated by a certain amount of Ah removed from the batteries or if the batteries reach a certain voltage level. The experimental voltage and consumed capacity profiles are shown in Fig. 6.

4.2. Evaluation on the NP model with different RC networks

For the difficulties to determine the minimum RC networks theoretically, a comparison of the terminal voltage estimation error between the model-based simulation and the experiment is conducted and the statistics of the estimation error is calculated. The results are listed in Table 1 for the NP model with $n = 0,1,2$. A detailed comparison of the estimation errors of the terminal voltage are shown in Fig. 7.

It can be seen that the estimation error of the terminal voltage is maximum for $n = 0$, decreases sharply for $n = 1$ compared with that for $n = 0$, and reduces gradually for $n = 2$ compared with that for $n = 1$. It concludes that the voltage relaxation effect of the $LiFePO_4$ battery module can not be ignored and one or two RC networks are reasonable for its dynamic modeling. Finally, the NP model with $n = 1$, $n = 2$ is selected for the online estimation of the SOC and the OCV to get a compromise between the model accuracy and the online calculation cost.

Table 1
The statistics list of the estimation error of the NP model.

n	Minimum/Maximum (V)	Mean (V)	Variance (V^2)
0	−0.2139/0.1116	−0.0414	9.6866e-004
1	−0.1394/0.0631	−0.0065	4.7054e-004
2	−0.0920/0.0301	−0.0061	2.4375e-004

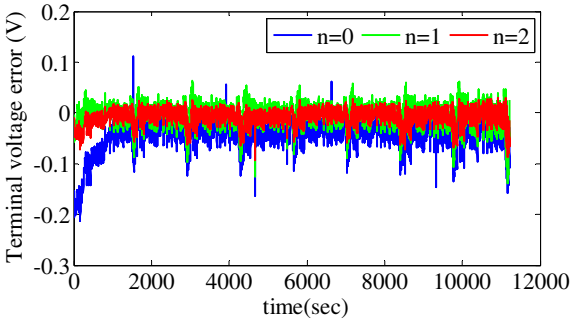

Fig. 7. The estimation error profiles of the terminal voltage of the NP model ($n = 0,1,2$).

4.3. Online identification results

In order to provide a comparison, the online identification of the model parameters are carried out according to Fig. 2 with $n = 0$, $n = 1$ and $n = 2$ respectively. The optimal forgetting factor λ equals 0.98 so as to pursue a good balance between the parameter tracking capability and misadjustment. A small $\boldsymbol{\theta}_n(0)$ and a large error covariance matrix $\boldsymbol{P}(0)$ are offered to initialize the identification algorithm.

With $n = 0$, the NP model is simplified as the Rint model and its model parameters are R_O and U_{OC}, the online identification results are shown in Fig. 8(a) and Fig. 8(b). It can be seen the R_O fluctuates as a function of SOC since it is the only component simulating the dynamic behavior and reflects the total equivalent resistance including the polarization impedance at some extend.

With $n = 1$, the NP model is simplified as the Thevenin model and its model parameters are U_{OC}, a_1, a_2, and a_3. The online identification results for a_1, a_2 and a_3 are shown in Fig. 9. And the U_{OC} and R_O is calculated with Eq. (8) and shown in Fig. 10.It can be seen that the online estimation of R_O and U_{OC} based on the Thevenin model are smoother than that based on the Rint model due to the Thevenin model simulates the batteries' dynamic behavior with the R_O and a RC network together. The R_O in Fig. 10(a) only simulates the batteries' ohmic resistance, its small fluctuation is due to the simplified method which using an equivalent circuit model to simulate the complicated chemical process of batteries.

With $n = 2$, the NP model is simplified as the dual polarization (DP) model and its model parameters are U_{OC}, b_1, b_2, b_3, b_4 and b_5.

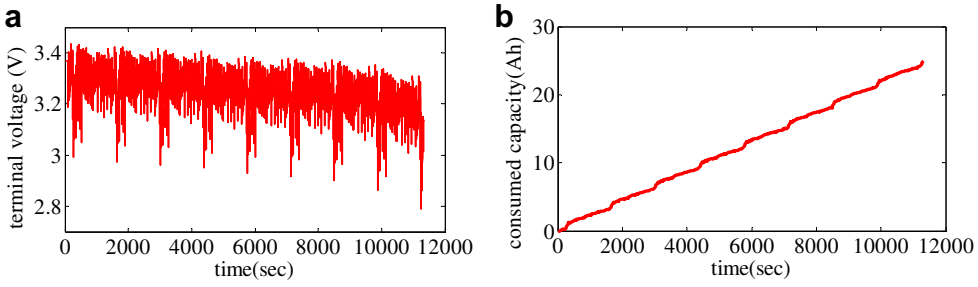

Fig. 6. The experimental terminal voltage and consumed capacity profiles of 9 UDDS cycles.

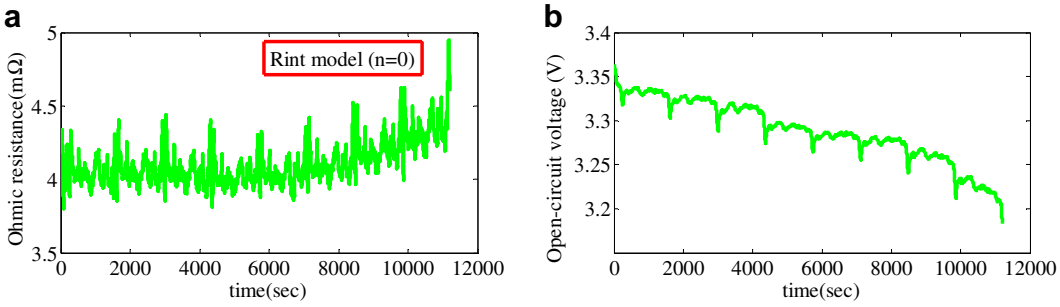

Fig. 8. The online identification result based on the Rint model: (a) ohmic resistance; (b) OCV.

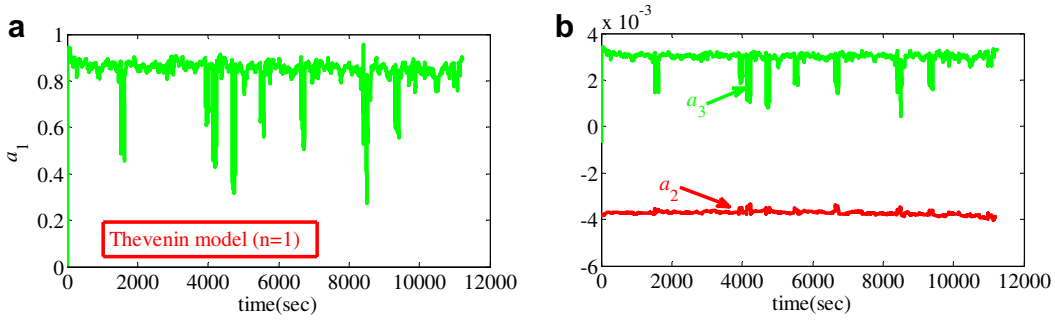

Fig. 9. The online identification results based on the Thevenin model: (a) a_1; (b) a_2 and a_3.

The online identification results for b_1, b_2, b_3, b_4 and b_5 are shown in Fig. 11. And the U_{OC} and R_O is calculated with Eq. (21) and shown in Fig. 12. It can be seen that the online estimation of R_O and U_{OC} based on the DP model are smoother than that based on the Rint model and the Thevenin model due to the DP model simulates the batteries' relaxation effect in more details. The R_O in Fig. 12(a) only simulates the batteries' ohmic resistance, its small fluctuation is due to the simplified method which using an equivalent circuit model to simulate the complicated chemical process of batteries.

The steady values of R_O and U_{OC} based on the Thevenin model and the DP model provide a foundation for the online SOC estimation.

5. Online model-based state-of-charge estimation

The online SOC estimation is realized by online identification of the OCV and the predetermined OCV-SOC lookup table based on the battery's intrinsic relationship between the SOC and the OCV. In order to build the relationship, a series experiments are purposely designed and the OCV is measured according to each SOC set point.

5.1. OCV-SOC lookup table by experimental approach

Electro-Motive Force (EMF) is a battery's internal driving force for providing energy to a load. The battery voltage only equals the EMF when no current flows and the voltage has relaxed to its equilibrium value, i.e. the OCV. Two OCV determination methods have been considered in [24]: linear interpolation and voltage relaxation. The voltage relaxation approach is the commonly used method to get the OCV-SOC map which keeps the battery in static state for enough long period under some specific SOC intervals (such as 10% SOC intervals in [9] and 4% in [24]). As a result, long time is consumed to get a perfect OCV-SOC curve. For the linear interpolation method, the average battery voltage, calculated at the same SOC, is inferred from the battery voltages during two

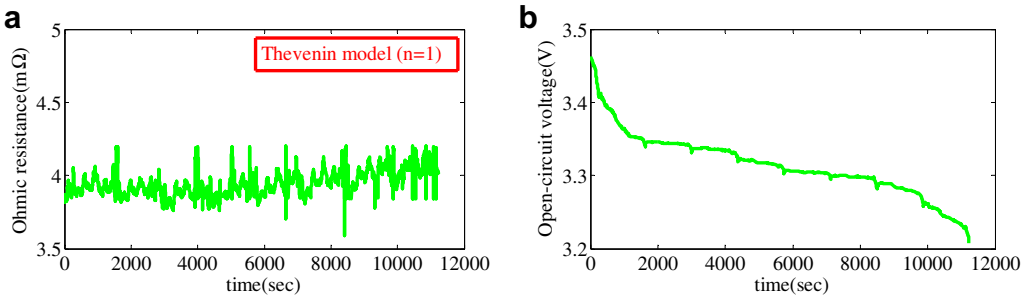

Fig. 10. The online identification results based on the Thevenin model: (a) R_o; (b) OCV.

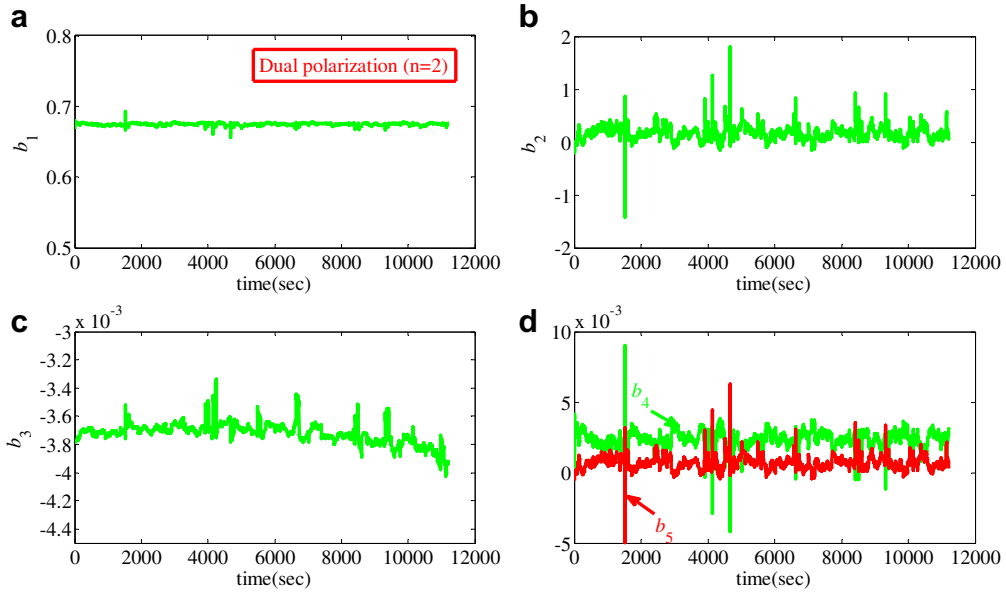

Fig. 11. The online identification results based on the DP model: (a) b_1; (b) b_2; (c) b_3; (d) b_4 and b_5.

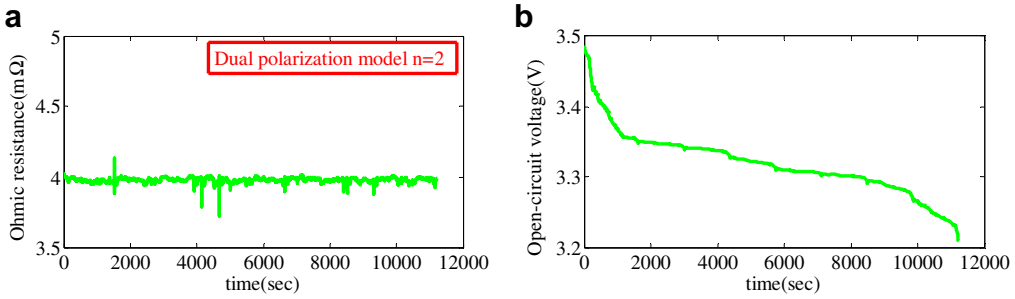

Fig. 12. The online identification results based on the DP model: (a) R_o; (b) OCV.

consecutive discharge and charge cycles with the same low C-rate current and temperature in order to minimize the possible effects of overpotential and hysteresis.

In this paper, the OCV is determined using the linear interpolation method, which comprises the following steps. First the battery module is fully charged at a constant current rate of C/9 [25] until its voltage reaches 3.6 V, and at the end of the charge cycle, the SOC level is defined to be 100%; Then a rest period of 16 h follows; After that, the battery is fully discharged at a constant current rate of C/9 until its voltage reaches 2.8 V, and at the end of the discharge cycle, the SOC level is defined to be 0%. The low current rate is chosen to minimize the effect of the overpotential. The long rest period is chosen to ensure that a new cycle would always start in the equilibrium state. By this way, a not-fully-relaxed voltage is eliminated from the OCV determination [24,26]. Fig. 13 shows the average OCV curve obtained at 25 °C using the linear interpolation method.

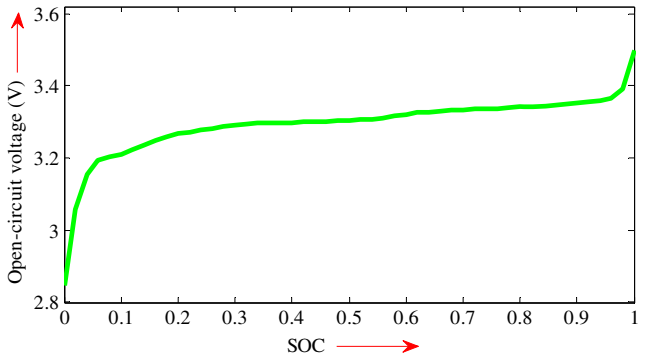

Fig. 13. The experimental OCV profiles.

5.2. Experiment result of the SOC estimation

The SOC estimation experiment is carried out with nine consecutive UDDS cycles. The results are shown in Fig. 14 based on the NP models with $n = 0,1,2$ and the SOC estimation errors between the estimations and the true values are also given in Fig. 14. A statistic analysis are shown in Table 2 correspondingly.

Table 2 shows the maximum is 0.04327, the mean is 0.01423 and the variance is 6.3e-004 for the absolute SOC estimation errors in case of $n = 2$. Fig. 14 and Table 2 indicate that a reasonable SOC estimation is realized with an acceptable accuracy and a good convergence with $n = 1$ and $n = 2$. A better SOC estimation will be achieved if the SoH of the battery based on the estimation result of R_O is considered. Also, those adaptive and robust algorithms'

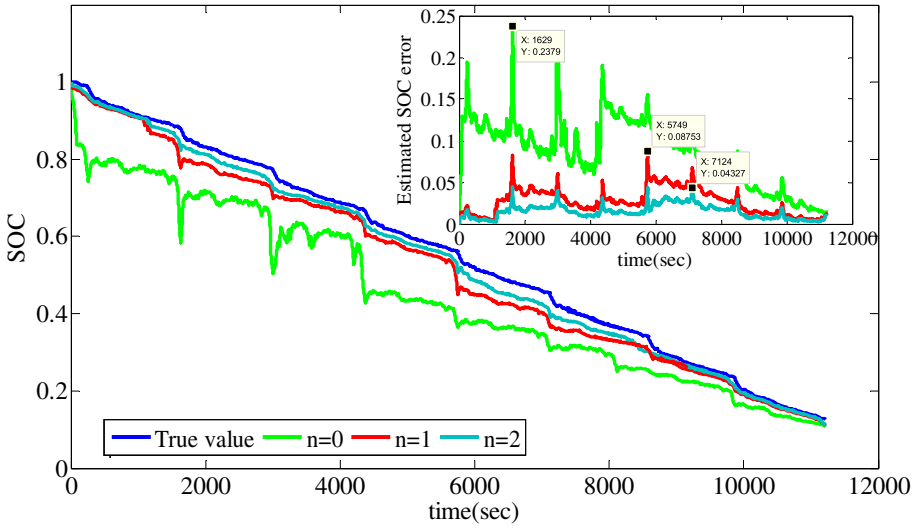

Fig. 14. The SOC estimation and its error curves based on the NP models (n = 0,1,2).

Table 2
The statistics list of the SOC estimation error of the NP models.

n	Maximum	Mean	Variance
0	0.23790	0.08126	6.2e-003
1	0.08753	0.01958	9.8e-004
2	0.04327	0.01423	6.3e-004

application will improve the accuracy of the SOC estimation further. That will be our next research focus.

6. Conclusions

An online model-based SOC estimation method is put forward theoretically and is verified experimentally. The main concluding remarks can be made below:

1) An equivalent circuit model with n RC networks, named the NP model, is reasonable for the necessary simulation of the polarization characteristic of lithium-ion batteries. By comparison, one or two RC networks are reasonable for the dynamic simulation of the $LiFePO_4$ battery module.
2) The equations for the NP model are built in the frequency domain. A recursive function is deduced for the online estimation of the OCV and R_O. A RLS algorithm with an optimal forgetting factor is applied to implement the online identification of the model parameters.
3) Two OCV determination methods, which are linear interpolation and voltage relaxation, were discussed. For the $LiFePO_4$ battery module, its relationship between the SOC and the OCV is built based on the experimental data with the linear interpolation method.
4) The experiments show that the online model-based SOC estimation is reasonable with an acceptable accuracy. For the absolute SOC estimation errors in case of $n = 2$, the maximum is 0.04327 for almost nine consecutive UDDS cycles.

Our future work will focus on a better online model-based SOC estimation by the additional consideration of the SoH (to compensate for the OCV's decrease) and the Kalman filter (to implement the online identification of the model parameters more accurately and efficiently) together with the OCV-SOC lookup table. Furthermore, we will use voltage relaxation method under different temperatures to get a more perfect OCV-SOC map for the SOC calibration in EVs.

Acknowledgments

This work was supported by the National High Technology Research and Development Program of China (2010AA112304) in part, the International Cooperation Research Program of Chinese Ministry of Science and Technology (2010DFB70090) in part, the National Natural Science Foundation of China (50905017) in part and also the research foundation of National Engineering Laboratory for Electric Vehicles in part.

References

[1] Wenhua HZ, Ying Z, Tatarchuk Bruce J. A simplified equivalent circuit model for simulation of Pb-acid batteries at load for energy storage application. Energy 2011;52:2794–9.
[2] Hongwen H, Song Y, Zhenjun X. Integrated control method for a fuel cell hybrid system. Asia-Pac J Chem Eng 2009;4:68–72.
[3] Fengchun S, Xiaosong H, Yuan Z, Siguang L. Adaptive unscented Kalman filtering for state of charge estimation of a lithium-ion battery for electric vehicles. Energy 2011;36:3531–40.
[4] Vasudeo V, Mohan A, Mohan K. Integrated battery controller for distributed energy system. Energy 2011;36:2392–8.
[5] Kuei-Hsiang C, Jing-Wei C. State-of-health estimator based-on extension theory with a learning mechanism for lead-acid batteries. Expert Syst Appl 2011;38:15183–93.
[6] Johnson VH. Battery performance models in ADVISOR. J Power Sources 2002; 101:321–9.
[7] Lijun G, Shengyi L, Roger AD. Dynamic lithium-ion battery model for system simulation. IEEE Trans Compon Pack Tech 2002;25:495–505.
[8] Caiping Z, Chengning Z, Jiangzhou L, Sharkh SM. Identification of dynamic model parameters for lithium-ion batteries used in hybrid electric vehicles. High Technol Lett 2010;16:6–12.
[9] Hongwen H, Rui X, Xiaowei Z, Fengchun S, Jinxin F. State-of-charge estimation of the lithium-ion battery using an adaptive extended kalman filter based on an improved Thevenin model. IEEE Trans Veh Tech 2011;60:1461–9.
[10] Hongwen H, Rui X, Jinxin F. Evaluation of lithium-ion battery equivalent circuit models for State of charge estimation by an experimental approach. Energies 2011;4:582–98.
[11] KongSoon N, Chin-Sien M, Yi-Ping C, Yao-Ching H. Enhanced coulomb counting method for estimating state-of-charge and state-of-health of lithium-ion batteries. Appl Energy 2009;86:1506–11.
[12] Hongwen H, Rui X, Hong-qiang G. Online estimation of model parameters and state-of-charge of LiFePO4 batteries in electric vehicles. Appl Energy 2012;89: 413–20.

[13] Lee SJ, Kim J, Lee J, Cho BH. State-of-charge and capacity estimation of lithium-ion battery using a new open-circuit voltage versus state-of-charge. J Power Sources 2008;185:1367–73.
[14] Windarko NA, Choi J. SoC estimation based on OCV for NiMH batteries using an improved Takacs model. J Power Electronics 2010;10:181–6.
[15] Windarko NA, Choi J. Hysteresis modeling for estimation of State-of-Charge in NiMH battery based on improved Takacs model. In Proc. 2009 International Telecommunications Energy Conf; 2009. 1–6.
[16] Roscher MA, Sauer DU. Dynamic electric behavior and open-circuit-voltage modeling of LiFePO4-based lithium ion secondary batteries. J Power Sources 2001;196:331–6.
[17] Jingyu Y, Guoqing X, Huihuan Q, Yangsheng X. Robust state of charge estimation for hybrid electric vehicles: Framework and algorithms. Energies 2010;3:1654–72.
[18] Alvin JS, Craig F, Pritpal S, Terrill A, David ER. Determination of state-of-charge and state-of-health of batteries by fuzzy logic methodology. J Power Sources 1999;80:293–300.
[19] Plett GL. Extended Kalman filtering for battery management systems of LiPB-based HEV battery packs – Part 3. State and parameter estimation. J Power Sources 2004;134:277–92.
[20] Harry M, Anthony B, Lawrence B, Robert B. Kalman filter estimation of monthly U.S. oil imports. Energy 1986;11:271–80.
[21] Shuai W, Lean Y, Ling T, Shouyang W. A novel seasonal decomposition based least squares support vector regression ensemble learning approach for hydropower consumption forecasting in China. Energy 2011;36(11): 6542–54.
[22] U.S. Environmental Protection Agency, EPA Urban Dynamometer Driving Schedule (UDDS). http://www.epa.gov/oms/standards/light-duty/udds.htm.
[23] Hongwen H, Rui X, Yuhua C. Dynamic modeling and simulation on hybrid power system for electric vehicle application. Energies 2010;3: 1821–30.
[24] Pop V, Bergveld HJ, Danilov D, Regtien PPL, Notten PHL. Battery management systems: accurate state-of-charge indication for battery-powered applications. London: Springer; 2008.
[25] Technical specification of Battery Management System for Electric vehicles. http://www.catarc.org.cn/Upload/file/bzyj/PDF/zhengqiuyijian-sc27-19-bzsm.pdf.
[26] Pop V, Bergveld HJ, Op het Veld JHG, Regtien PPL, Danilov D, Notten PHL. Modeling battery behavior for accurate state-of-charge indication. J Electrochem Soc 2006;153:A2013–22.